Smoking gun for thallium geochemistry in volcanic arcs: Nataliyamalikite, TlI, a new thallium mineral from an active fumarole at Avacha Volcano, Kamchatka Peninsula, Russia

Victor Okrugin[1], Michael Favero[2], Amelia Liu[2], Barbara Etschmann[2], Ekaterina Plutachina[1], Stuart Mills[3], Andrew G. Tomkins[2], Mariaya Lukasheva[4], Vladimir Kozlov[5], Svetlana Moskaleva[1], Mikhail Chubarov[1], and Joël Brugger[2,*]

[1]Institute of Volcanology and Seismology, Russian Academy of Science, Petropavlovsk-Kamchatsky, 683 006, Russia
[2]School of Earth, Atmosphere and the Environment, Monash University, Clayton, 3800, Australia
[3]Geosciences, Museum Victoria, GPO Box 666, Melbourne 3001, Victoria, Australia
[4]Tescan Ltd., Grazhdansky pr.11, St. Petersburg 195220, Russia
[5]Oxford Instruments Overseas Marketing Ltd., Moscow Office, Denisovskii pr. 26, Moscow, 105005, Russia

Abstract

This paper describes the new mineral nataliyamalikite, the orthorhombic form of thallium iodide (TlI), from high-temperature fumaroles from the Avacha volcano, Kamchatka Peninsula, Russia. We also present some chemical analyses showing extreme enrichment of Tl in the volcanic gases at the Avacha volcano, and a review of thallium geochemistry that highlights the fascinating processes that led to the formation of nataliyamalikite.

Nataliyamalikite occurs as pseudo-cubic nanocrystals (≤0.5 μm) within vacuoles in an As-(Te)-rich amorphous sulfur matrix and rarely as irregularly shaped aggregates up to ~50 μm in diameter within the amorphous sulfur matrix. Associated minerals include an unidentified Tl-As-S mineral, barite, and rare inclusions of a Re-Cu-bearing phase. The mean empirical composition based on four EDS analyses is $Tl_{1.00}(I_{0.95}Br_{0.03}Cl_{0.02})$, corresponding to the ideal formula TlI. Nataliyamalikite crystallizes in the orthorhombic system, space group *Cmcm*, which is consistent with the low-temperature (<175 °C) synthetic TlI polymorph. EBSD data reveal that some grains retain the cubic symmetry ($Pm\overline{3}m$) of the high-temperature polymorph, although most analyzed grains display the orthorhombic symmetry. Single-crystal X-ray studies of material extracted by the focused ion beam-scanning electron microscopy (FIB-SEM) technique, and carried out on the MX2 macromolecular beamline of the Australian Synchrotron, determined the following cell dimensions: $a = 4.5670(9)$, $b = 12.803(3)$, $c = 5.202(1)$ Å, $V = 304.2(1)$ Å^3, and $Z = 4$. The six strongest calculated X-ray reflections and their relative intensities are: 3.31 (100), 2.674 (73), 3.20 (43), 2.601 (28), 2.019 (21), and 2.284 Å (19). The combination of EBSD analysis (providing an efficient test of the crystallinity and crystal symmetry of a population of micrometer-sized grains) and synchrotron single-crystal X-ray micro-diffraction (beam size ~7.5 μm) on micro-aggregates extracted using FIB-SEM opens the way to the characterization of challenging specimen—in this case, the sulfur matrix is highly beam sensitive, and the nataliyamalikite grains could not be isolated using optical microscopy.

The high-temperature (>600 °C) sulfidic (~1.2 wt% S) vapors at Avacha are extremely enriched in thallium; with 34 ppm, they contain an order of magnitude more Tl than the richest volcanic gases analyzed to date and ~100× more Tl than most metal-rich fumarolitic fluids associated with volcanic arcs. The formation of nataliyamalikite illustrates the complex processes that control thallium geochemistry in magmatic arc systems. Thallium minerals have now been reported in andesitic (Avacha), basaltic (Tolbachik, Kamchatka), as well as rhyolitic (Vulcano, Eolian Islands, Italy) volcanoes. Ultimately, these thallium minerals result from the transfer of thallium from subducted sediments to volcanic gases in arc volcanoes. We suggest that the extremely thallium-enriched vapors from which nataliyamalikite formed result from complex and transient interactions between Tl-rich sulfosalt melts and magmatic vapors, a process that may be important in controlling metal distribution in boiling epithermal systems.

Keywords: Nataliyamalikite, new mineral, thallium, fumaroles, vapor transport, Avacha Volcano, Kamchatka Peninsula, Russia

Introduction

Thallium (Tl) is a toxic heavy metal that has an upper crustal abundance of 550 ppb, comparable to that of Mo (600 ppb) and Bi (230 ppb) (Hu and Gao 2008). Yet, minerals containing Tl as an essential element are scarce, mainly because Tl(I) can behave both as a chalcophile element, substituting for example for Pb(II), or as lithophile element, in which case it substitutes for K(I). As a result, exceptional processes are required to form Tl minerals (Christy 2015). In this paper, we describe a new locality with

* E-mail: joel.brugger@monash.edu

1736

Tl-dominant mineralogy, including the new mineral nataliyama-likite, TlI. Nataliyamalikite forms in high-temperature fumaroles at the Avacha andesitic stratovolcano, Kamchatka Peninsula, Russia. This represents the third occurrence of Tl minerals associated with fumarolitic activity in arc volcanoes. The aim of this paper is to provide a formal description of nataliyamalikite as a new mineral, as well as an overview of the processes that give rise to high local concentrations of Tl, leading to the formation of exotic Tl-minerals.

NATALIYAMALIKITE, A NEW MINERAL

Occurrence

Nataliyamalikite occurs at the Avacha volcano, on the Kamchatka Peninsula, Far Eastern Russia (53°15′18″N, 158°49′48″E), in association with active high-temperature (to 620–640 °C) fumarolic vents (Fig. 1). The Avacha (or Avachinsky) volcano lies 25 km NE of Petropavlovsk–Kamchatka, the largest city on the Peninsula.

The Kamchatka Peninsula is one of the longest-lived volcanically active areas on the planet, with activity dating back to the Late Triassic (Bindeman et al. 2002; Pedoja et al. 2006; Waltham 2001). Holocene volcanic products comprise basalts, basaltic andesites, andesites, basaltic trachyandesites, trachyandesites, trachyte/trachydacites, dacites, and rhyolites (Viccaro et al. 2012). The Avacha volcano is one of the most active volcanoes on the Kamchatka Peninsula, and began erupting in the middle to late Pleistocene era. The Avacha volcano is of the Somma–Vesuvius type, with a base ~4 km in diameter. The active cone is located in a horseshoe-shaped caldera (~2300 m altitude), which formed 30 000–40 000 years ago in a major landslide, which covered an area of 500 km^2 south of the volcano (Levin et al. 2004; Taran et al. 1997; Waltham 2001). The active cone began rising ~5000 years ago and currently sits on the SE border of the Somma caldera, resulting in an asymmetrical appearance with respect to the center of the caldera (Koulakova et al. 2014). The Young Cone is 2741 m in altitude, with a summit crater ~350 m wide.

Magmatism at the volcano displays a range of products, typically classified as basalts, basaltic andesites, and andesites. The most recent large eruption (VEI = 4) occurred in 1945, when about 0.25 km^3 of magma was ejected. The volcano has since had small eruptions in 1991 and 2001 (Ivanov et al. 1996; Melekestsev et al. 1994; McGimsey et al. 2004; Viccaro et al. 2012), shaping the modern morphology and fumarolitic activity (Fig. 1a). The products of the 1991 effusive activity generally have basaltic andesite compositions. Lava filled the ~175 m deep 1945 crater before overflowing on the southern and southeastern flanks of the young cone (Fig. 1a). The minor 2001 eruption started on October 5 by a small steam and ash explosion in the summit area (McGimsey et al. 2004). On October 17, a helicopter observed a new fracture, cutting east-southeast–west-northwest across the 1991 lava flow that had filled a pre-existing summit crater, and extending another 100–150 m down the flank of the cone. Significant fumarolic activity and sulfur deposition was noted at the intersections of the fracture and the edifice (McGimsey et al. 2004). This fumarolic activity is ongoing to this day (Fig. 1a). Nataliyamalikite occurs in deposits associated with high-temperature fumarolic vents along the 2001 fracture (Figs. 1a and 1b), as a minor component in a
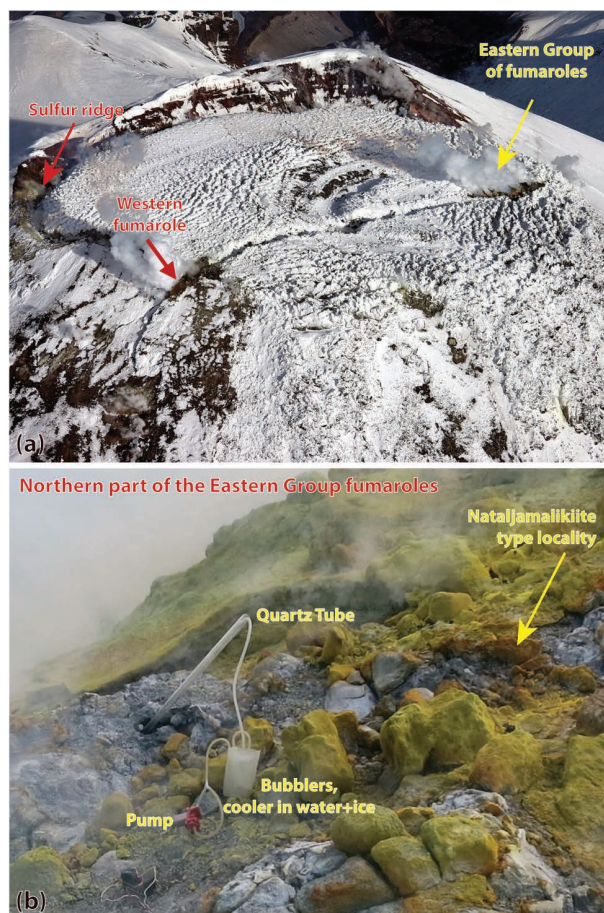
FIGURE 1. The occurrence of nataliyamalikite at the Avacha Volcano, Kamchatka, Russia. (**a**) Aerial view of the somma and associated fumarole field. The 1991 lava flow fills the summit crater and spills over the south-southwest rim. The 2001 fracture, steaming profusely at both ends, cuts across the surface of the 1991 lava flow (McGimsey et al. 2004). (**b**) Close view of the sample locations. Nataliyamalikite was found both in natural sublimates near high-T fumaroles and in quartz tubes placed within the fumaroles. (Color online.)

bright orange, X-ray amorphous, As-rich (~20 mol% As) S-rich coating on lava and scoria around the vents.
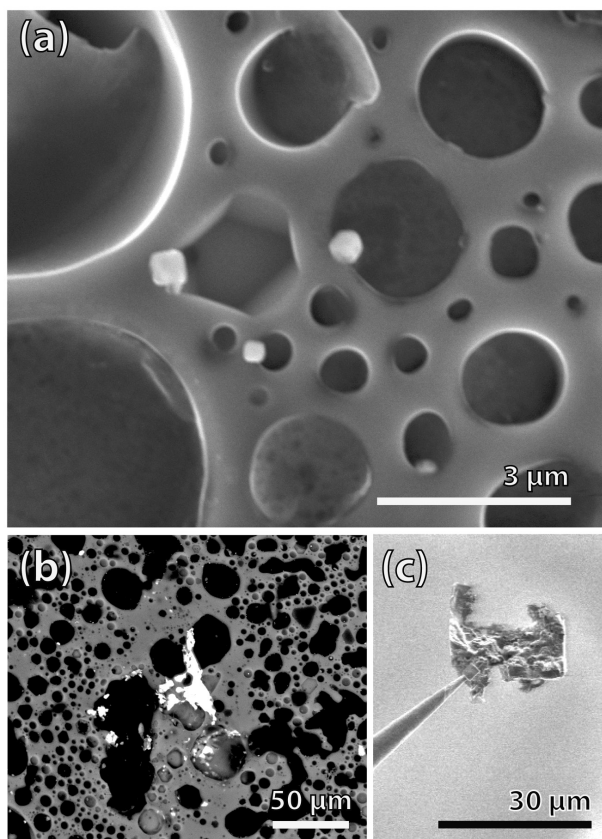
Name and type material

The mineral is named for Natalja Alexandrovna Malik (Н.А. Малик) (born March 24, 1981). Malik graduated at the Kaliningrad State University (specialization geoecology). Since 2004, she has been a researcher at the Institute of Volcanology and Seismology of the Far Eastern Branch of The Russian Academy of Sciences in Petropavlovsk–Kamchatsky, Russia. Her main interests revolve around the study of fumarolic activity, volcanic gases, explosive eruptions, tephra, and ash leachates. She has published 12 publications in peer-reviewed journals (e.g., Moiseenko and Malik 2014; Zelenski et al. 2014). One holotype specimen is deposited in the collections of the Museum Victoria, Melbourne, Australia, catalog number M53602. The mineral and name have both been approved by the IMA Commission on New Minerals and Mineral Names (IMA2016-022).

Physical and optical properties

Nataliyamalikite (Russian Cyrillic: НАТАЛИЯМАЛИКИТ) occurs most widely as pseudo-cubic nanocrystals (≤0.5 μm) within vacuoles in an As-rich, X-ray amorphous, sulfur-rich matrix (Fig. 2a). A few crystals were observed on mascagnite [(NH$_4$)$_2$SO$_4$] balls (Fig. 3). Rarely, larger, irregularly shaped aggregates up to ~50 μm in diameter occur in vacuoles or within the S-rich matrix (Fig. 2b). In some of these aggregates, nataliyamalikite appears to be intergrown at micrometer scale with an unidentified Tl-As-S mineral. Other associated minerals include barite and rare inclusions of a Re-Cu-bearing phase (1–3 μm in size). The silica associated with the S-(As)-rich crusts contains rare inclusions (~1 μm) of native (Te,Se).

Color (macroscopic), streak, luster, hardness, cleavage, fracture, and parting could not be observed due to the size of the mineral grains, their scarcity within the samples, and their occurrence in a dark orange, translucent matrix of amorphous arsenian sulfur. The synthetic analog is yellow, but is photosensitive and blackens readily upon exposure to light. In reflected light, the color is medium gray; internal reflections could not be observed, again because the small grains are embedded in yellow to dark orange arsenian sulfur. Density could not be measured because there is insufficient material available. Density calculated based on the ideal TlI formula and the unit cell from the single-crystal X-ray data (see below) is 7.23 g/cm^3.
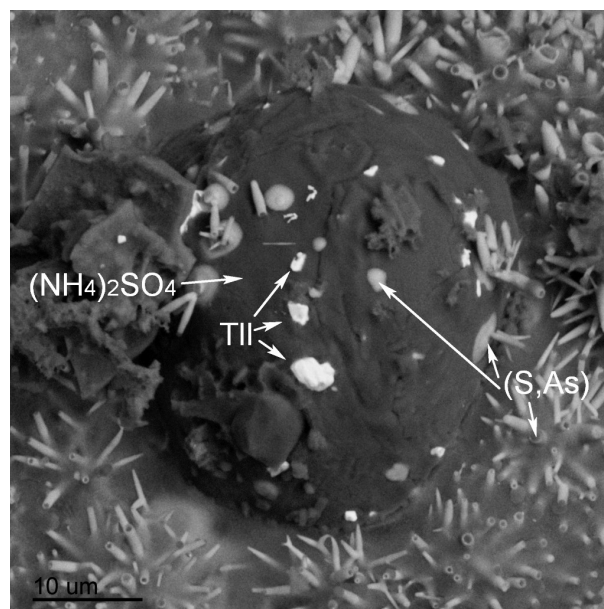
Chemical composition

Analysis of the material is challenging, as a result of the combination of: (1) the small size of single crystals; (2) the composite nature of the larger aggregates; and (3) the extreme beam sensitivity of both the mineral and the surrounding matrix. We present four analyses (Table 1) from different grains obtained using standard-free analysis on a Tescan Lyra FIB-SEM equipped with an Oxford Instruments Aztec Synergy system X-Max 150 mm^2 EDS detector. Operating conditions were: no tilt, accelerating voltage 10 kV, and beam current 0.5 nA. The empirical formula based on 2 apfu is Tl$_{1.00}$(I$_{0.95}$Br$_{0.03}$Cl$_{0.02}$). The theoretical composition has 61.69 wt% Tl and 38.31 wt% I.

Room-temperature electron backscatter diffraction (EBSD)

There are two well-established polymorphs of TlI (Table 2). According to the phase diagram of Brightwell et al. (1983), at ambient pressure the low-temperature orthorhombic modification is stable at <175 °C, and the cubic form with caesium chloride structure is stable at T >175 °C. Note that the cubic form is also thermodynamically stable at high pressure (e.g., above ~3 kbar at 20 °C; Samara et al. 1967). Shamovskii and Shushkanov (1968) proposed a NaCl-type structure for high-T TlI (>175 °C) (ICSD#60491; Table 2), but this has not be validated by subsequent studies.

We used EBSD (Fig. 4) to distinguish between the cubic and orthorhombic forms in the type specimen, to verify that the orthorhombic form identified by the single-crystal X-ray diffrac-

FIGURE 2. SEM images showing the occurrence of nataliyamalikite in the natural fumarole deposits at Avacha. (a) High-resolution image of an unpolished sample, showing occurrence of pseudo-cubic nanocrystals of nataliyamalikite within vacuoles in an As-(Te)-rich sulfur matrix. Secondary electron mode, 10 keV. (b) Rare larger aggregates of nataliyamalikite within the arsenian sulfur matrix. Backscattered electron image, 25 keV. (c) FIB composite nataliyamalikite/matrix fragment used for the single-crystal analysis, mounted on tungsten needle (ion image).

FIGURE 3. Nataliyamalikite grains on mascagnite, (NH$_4$)$_2$SO$_4$.

tion study is indeed the polymorph present in the sample at ambient conditions. This is important since the crystal structure was determined at 100 K on a micro-crystal extracted via FIB. The EBSD measurements were carried out on two different samples at the Monash University Centre of Electron Microscopy, Australia (A); and at the Tescan Russia demonstration laboratory, St. Petersburg, Russia (B). Both samples unambiguously contained the orthorhombic modification (Table 3). While EBSD data could be collected on two grains with the orthorhombic structure at Monash, Tescan Labs identified two grains with a cubic crystal structure alongside two grains with the orthorhombic crystal structure. Table 3 shows the goodness of fit parameters for the four crystals on which good data could be obtained, demonstrating an orthorhombic crystal structure.

The following instruments and analytical conditions were used in Melbourne (A) and Moscow (B). (A) Quanta 3DFEG equipped with a 10 mm² SDD EDAX Pegasus detector and a TSL Hikari EBSD system. Analytical conditions for EDS mapping were 10 kV accelerating voltage and 8 nA beam current. Conditions for EBSD were 20 keV accelerating voltage and 16 nA beam current. Grains were polished using a 5 keV, 2.3 nA

Ga^+ ion beam at a 6° glancing angle to improve surface crystallinity and obtain good quality EBSPs. (B) Tescan Lyra 3 GM with Ga ion gun equipped with an Oxford Instruments Aztec Synergy system with X-Max 150 mm² EDS detector and a NordlysMax EBSD camera. Analytical conditions for EDS mapping were no tilt, acceleration voltage of 10 kV, and a beam current of 0.5 nA. A protective and conductive Pt layer (ca. thickness 100 nm) was applied before milling and polishing for EBSD analysis. FIB milling was done at a tilt –7° to ion gun, at 30 kV for milling and 5 kV for polishing. The EBSD patterns were collected with a tilt of 77° at 20 kV and 0.5 to 1 nA currents.

Microsampling

The size of the nataliyamalikite aggregates (mostly <30 μm; Figs. 2 and 3) and the fact that they are nearly invisible under optical microscopy necessitated an appropriate method to obtain material for crystal structure determination. A 20 × 10 × 2 μm³ fragment consisting of a fine mixture of nataliyamalikite and amorphous arsenian sulfur was cut from a polished section using a focused Ga^+ ion beam SEM (FIB-SEM), following the method of Ciobanu et al. (2014). The extracted foil (Fig. 2c) was transferred onto a nylon micro-loop for single-crystal data collection.

Single-crystal X-ray study at 100 K

The single-crystal study was carried out at the macromolecular beamline MX2 of the Australian Synchrotron (Table 4). The

TABLE 1. Analytical data (in wt%) for nataliyamalikite (n = 4), compared to lafossaite

Constituent	Mean	Range	S.D.	Lafossaite[c]
Tl	61.40	61.07–62.01	0.4	81.74(1.49)
I	36.00	32.65–37.33	2.2	
Br	0.65[a]			5.99(0.28)
Cl	0.21[a]			10.79(0.57)
As[d]		0.64–1.42		
Al[d]		0.76, 0.91		
Si[d]	1.00[a]			
Total	98.30[b]	100.0–101.1		

[a] Detected in a single point.
[b] Taking into account only structural elements.
[c] From Roberts et al. (2006).
[d] Contamination from matrix.

TABLE 3. Summary of EBSD Mean Angle Deviation (MAD) for nataliyamalikite (orthorhombic, CMCM; structure from Helmholz 1937)

Grain no./Instrument	1/A	2/A	3/B	4/B
MAD (°)	0.9	0.49	0.31	0.58

Notes: Instrument: A = Quanta 3DFEG equipped with a 10 mm² SDD EDAX Pegasus detector. B = Tescan Lyra 3 GM with Ga ion gun equipped with an Oxford Instruments Aztec Synergy system with X-Max 150 mm² EDS detector. See text for details.

TABLE 2. Unit-cell data for polymorphs of Tll

Orthorhombic, "yellow form", "Lt"; Helmholz (1937)	$T < 175$ °C	orthorhombic	$Cmcm$	$a = 4.57(2)$ Å, $b = 12.92(1)$ Å, $c = 5.24(2)$ Å; 309(3) Å³
Caesium chloride, "red form"; Samara et al. (1967)	$T > 175$ °C	cubic	$Pm\bar{3}m$	$a = 4.2099(3)$ Å (at 20 °C, extrapolated from measurements 150–295 °C)
Cubic, "Ht", Shamovskii and Shushkanov (1968)	$T > 175$ °C	cubic	$Fm\bar{3}m$	$a = 6.94$ Å
Caesium chloride-type, "red form"; Blackman and Khan (1960)[a]	$T \leq 15$ °C[a]	cubic	$Pm\bar{3}m$	$a = 4.205$ Å (15 °C)

[a] Vapor deposited on amorphous base.
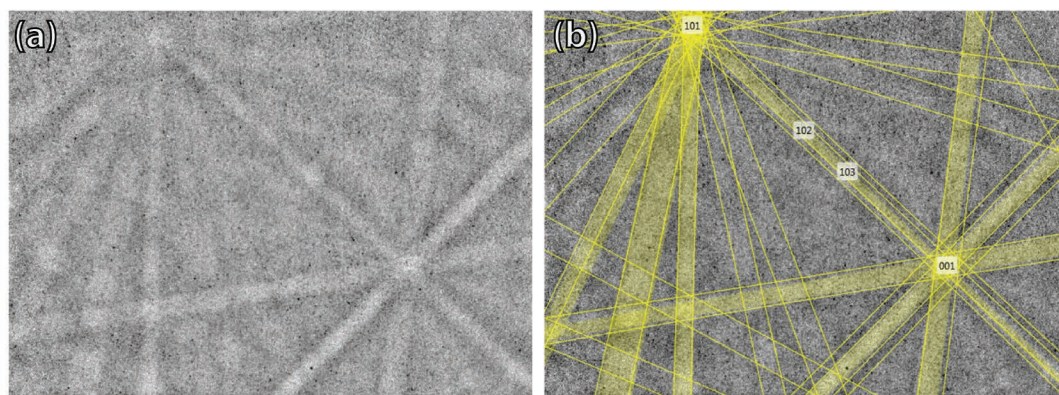
FIGURE 4. Example EBSD patterns. (**a**) Raw pattern. (**b**) Indexed pattern. (Color online.)

beam diameter was reduced to 7.5 μm using a collimator. The location of the measurement spot on the $20 \times 10 \times 2$ μm^3 FIB cut was selected on the basis of EDS spectra; the chosen point shows mainly Tl with little As contamination (the EDS detector has a thick window and is not sensitive to S and I). Data were collected using an ADSC Quantum 315r 2D detector and monochromatic radiation with a wavelength of 0.71086 Å. The crystal was maintained at 100 K in an open-flow nitrogen cryostream.

A φ scan was employed with frame widths of 1° and a counting time per frame of 1 s. The intensity data sets were processed using XDSauto and SADABS. Both atoms were found using SHELXS-97 (Sheldrick 2008), and then refined anisotropically using SHELXL-97 (Sheldrick 2008). The final model converged to $R_1 = 4.01\%$ for 268 reflections with $F_o > 2\sigma(F)$.

The measured crystal is orthorhombic, space group $Cmcm$ with the unit-cell parameters: $a = 4.5670(9)$ Å, $b = 12.803(3)$ Å, $c = 5.202(1)$ Å, $V = 304.2(1)$ Å^3, and $Z = 4$ (Table 4). Table 5 shows the calculated powder XRD pattern based on the results of the structure refinement of the natural phase, compared with existing data on the synthetic equivalent from the PDF database.

Crystal structure

The crystal structure of nataliyamalikite has only two atoms in the asymmetrical unit (Table 6; Fig. 5). Both atoms occupy a $4c$ special position $(0, y, \frac{1}{4})$. The structure is considered to be a distorted version of rock salt, where every anion is surrounded by eight cations and has cubic coordination geometry. Tl and I atoms have similar coordination environments. The full Tl (and I) coordination can be described as 1+4+2, where Tl atoms are coordinated by four iodide at ~3.4819(18) Å in a slightly out-of-plane square planar configuration, with one additional iodide ion at 3.3067(15) Å in an axial position. The opposite axial position is occupied by the Tl(I) lone electron pair (Brugger et al. 2016), and two more distant iodine atoms (3.846 Å) located on the same side as the Tl lone pair are weakly but significantly bonded. The Tl–Tl distance is 3.7603(12) Å. Slight corrugation of the

Tl-I layers lying parallel to (040) causes the shortest interlayer distances I⋯I to be 4.340 Å, while Tl⋯Tl distances are short at 3.760 Å, implying that there are attractive dipole-dipole interactions between lone pairs across the interlayer. This structure is also formed by NaCl and NaBr at very high pressures (~30 GPa), with short dipole⋯dipole interactions between the large, polarizable anions (Léger et al. 1998). Isopuntal compounds such as CrB can have much stronger bonding interactions between like atoms across the "interlayer" (zigzag B-B chains with B-B = 1.74 Å, Kiessling 1949).

Relation to other species

Nataliyamalikite is chemically related to lafossaite Tl(Cl,Br) [$Pm\overline{3}m$; $a = 3.8756(3)$ Å, $V = 58.213(8)$ Å^3, and $Z = 1$] from

TABLE 4. Data collection and structure refinement details for nataliyamalikite

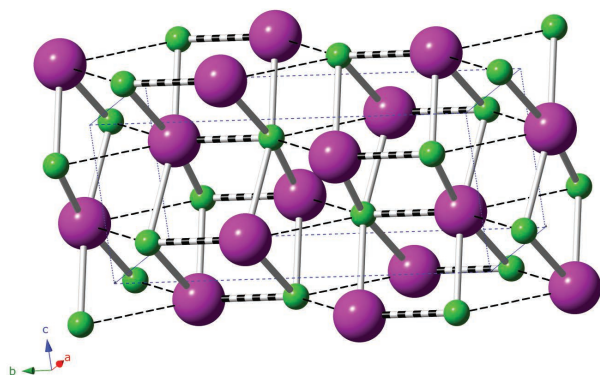|	
Diffractometer	ADSC Quantum 315r detector
Radiation	synchrotron (λ = 0.71086 Å)
Temperature	100(2) K
Structural formula	TlI
Space group	$Cmcm$
Unit-cell dimensions	$a = 4.5670(9)$ Å
	$b = 12.803(3)$ Å
	$c = 5.202(1)$ Å
V	304.2(1) Å^3
Z	4
Absorption coefficient	62.9 mm^{-1}
$F(000)$	536
θ range	3.18 to 29.99°
Index ranges	$-6 \le h \le 6, -17 \le k \le 17, -7 \le l \le 7$
Refls collected/unique	2869/272; $R_{int} = 0.056$
Reflections with $F > 2\sigma(F)$	268
Refinement method	Full-matrix least-squares on F^2
Parameters refined	10
GoF	1.227
Final R indices [$F_o > 2\sigma(F)$]	$R_1 = 0.0401, wR_2 = 0.0887$
R indices (all data)	$R_1 = 0.0410, wR_2 = 0.0894$
Largest diff. peak/hole	+6.37/−2.42 e/Å^3

$^a R_{int} = \Sigma|F_o^2 - F_o^2(\text{mean})|/\Sigma[F_o^2]$. GoF = $S = \{\Sigma[w(F_o^2 - F_c^2)^2]/(n-p)\}^{1/2}$. $R_1 = \Sigma||F_o| - |F_c||/\Sigma|F_o|$. $wR_2 = \{\Sigma[w(F_o^2 - F_c^2)^2]/\Sigma[w(F_o^2)^2]\}^{1/2}$; $w = 1/[\sigma^2(F_o^2) + (aP)^2 + bP]$ where a is 0, b is 394.6636, and P is $[2F_c^2 + \text{Max}(F_o^2,0)]/3$.

TABLE 5. Powder diffraction data for nataliyamalikite calculated from the crystal structure, compared to PDF# 74-1056

			Calculated from the crystal structure refinement (CrystalDiffract6)		PDF# 74-1056 Cell a = 5.24 Å; b = 4.57 Å; c = 12.92 Å	
h	k	l	d_{calc} (Å)	I/I_{max}	d_{meas} (Å)	I/I_{max}
0	2	0	6.40	2.3	6.46	2.4
1	1	0	4.30	10.8	4.31	8.6
0	2	1	4.04	8.1	4.07	6.6
1	1	1	3.31	100.0	3.33	100
0	4	0	3.20	43.0	3.23	44.3
1	3	0	3.12	0.4	3.13	0.4
0	4	1	2.726	9.6	2.749	7
1	3	1	2.674	73.1	2.689	69.5
0	0	2	2.601	28.1	2.620	26.9
0	2	2	2.410	0.4	2.427	0.3
2	0	0	2.284	18.8	2.285	17.3
1	5	0	2.234	6.9	2.249	5
1	1	2	2.226	3.9	2.238	3.2
2	2	0	2.151	0.3	2.153	1.1
0	6	0	2.134	1.0		
1	5	1	2.052	11.4	2.067	11.9
					2.034	20.5
0	4	2	2.019	21.4	2.010	0.3
1	3	2	1.997	0.2	1.992	2
2	2	1	1.988	2.4		
2	4	0	1.859	16.1	1.865	14.9
2	4	1	1.751	4.6	1.757	2.9
2	0	2	1.716	14.2	1.722	12.6
					1.711	1.8
					1.706	4.4
1	7	0	1.698	2.1	1.686	0.5
1	5	2	1.694	5.4		
0	2	3	1.674	0.7	1.663	0.8
2	2	2	1.657	0.2	1.626	12.1
1	7	1	1.614	12.6	1.618	9.5
1	1	3	1.608	10.0	1.615	7.7
0	8	0	1.600	2.7		
2	6	0	1.559	0.7	1.567	0.5
0	8	1	1.530	4.6	1.543	3.1
0	4	3	1.525	1.4	1.536	1.1
1	3	3	1.515	10.7	1.519	14
2	4	2	1.512	14.9	1.501	0.3
3	1	1	1.452	6.7	1.453	5.7
1	7	2	1.422	2.1	1.432	1.3
3	3	1	1.382	7.3	1.385	6.3
1	5	3	1.370	2.5	1.379	2.9
0	8	2	1.363	2.8	1.374	3.3

TABLE 6. Atom coordinates and displacement parameters (Å^2) for nataliyamalikite

	x/a	y/b	z/c	U_{11}	U_{22}	U_{33}
Tl	0.50	0.60605(6)	0.75	0.0200(5)	0.0173(5)	0.0190(5)
I	0.50	0.86433(9)	0.75	0.0167(6)	0.0148(6)	0.0172(6)

Note: U_{23}, U_{13}, U_{12} set to zero (site symmetry constraint).

Vulcano, Italy (Roberts et al. 2006). Both minerals form from high-temperature fumaroles on active volcanoes. The limited incorporation of I in lafossaite and of Cl in nataljamalikite (Table 1) reflects the large difference in size between the anions, with the crystal structure of nataliyamalikite favoring the large iodide ion. Note that a thallium chloride phase was identified on the basis of qualitative EDS analyses as equant inclusions 1–12 μm in diameter within polycrystalline diamonds from the Udachnaya kimberlite pipe (Yakutia, Russia), together with Cr spinel, native iron, native chromium, native copper, and native tantalum (Gorshkov et al. 1998). The other known thallium

halide minerals are steropesite, Tl_3BiCl_6 [Cc; a = 26.686(5) Å, b = 15.127(3) Å, c = 13.014(3) Å, β = 108.11(2)° and V = 4993(2) Å^3; Demartin et al. 2009], and hephaistosite, $TlPb_2Cl_5$ [$P2_1/c$; a = 8.9477(6) Å, b = 7.9218(7) Å, c = 12.4955(5) Å, β = 90.092(4)°, and V = 885.70(7) Å^3; Campostrini et al. 2008] both from the high-temperature fumaroles from Vulcano, Italy; and chrysothallite, $K_6Cu_6Tl(III)Cl_{17}(OH)_4\cdot H_2O$ [$I4/mmm$, a = 11.3689(7) Å, c = 26.207(2) Å, V = 3387.3(4) Å^3] from the second scoria cone of the Northern Breakthrough of the Great Tolbachik Fissure Eruption, Tolbachik volcano, Kamchatka, Russia; the latter mineral contains Tl(III) rather than Tl(I), and results from interactions involving high-temperature sublimate minerals, fumarolic gas and atmospheric water vapor at temperatures ≤150 °C (Pekov et al. 2015).

THALLIUM CONCENTRATIONS IN FUMAROLITIC VAPORS

Thallium is a volatile element in high-temperature magmatic hydrothermal systems (Henley and Berger 2013). Table 7 shows the measured Tl concentrations reported from several geothermal waters and fumarolitic vapors, compared to the other volatile metals Cd and Pb, as well as to Rb [Rb(I) has the same ionic radius as Tl(I), i.e., 1.61 vs. 1.59 Å in eightfold coordination, Shannon 1976]. Many localities show measurable Tl concentrations <20 ppb; concentrations above 100 ppb are rare, and were reported from single samples from Kudryavy Volcano (Kuril Islands; 140 ppb) and Mutnovsky volcano (Kamchatka; 110 ppb). Recently, the vapors emitted from the 2012–2013 Tolbachik eruption were shown to contain an order of magnitude more Tl (1470–1700 ppb) than geothermal waters and fumarole fluids by two independent studies (Zelenski et al. 2014; Chaplygin et al. 2016). There is no correlation among the Tl and Rb concentrations reported in Table 7, but high-Pb and -Cd contents generally correspond to high-Tl contents.

FIGURE 5. The crystal structure of nataliyamalikite. Thallium(I) in green, and iodine(-I) in purple. Thallium atoms are coordinated by 4 iodide ions at 3.4819(18) Å in slightly out-of-plane square planar configuration (rendered solid bonds), with one additional iodide ion at 3.3067(15) Å in axial position (rendered stripped bonds); the opposite axial position being occupied by the thallium(I) lone electron pair, with two weakly bonded iodide ions at 3.846(2) Å around the lone electron pair (dashed lines). (Color online.)

TABLE 7. Concentrations of thallium and a few geochemically related elements in selected geothermal waters and fumarolic gas condensates

Sample description	T (°C)	Tl (ppb)	Rb (ppb)	Pb (ppb)	Cd (ppb)	Reference
Seawater	2	0.014	120	0.0021	0.067	Li (1991)
East Pacific Rise vent fluids (average)	~350	6.5	n/a	63.8	9	Hannington et al. (2016)
Deep chloride waters from wells, New Zealand	195–320	0.4–15	n/a	<0.1–808	<0.1–13.3	Simmons et al. (2016)
Ohaki hydrothermal pool, New Zealand	95	0.3	n/a	n/a	n/a	Weissberg (1969)
Broadlands drill core 2, New Zealand	294 (max)	7	n/a	n/a	n/a	Weissberg (1969)
Champagne Pool, New Zealand	75	0.027	1170	<0.1	<0.029	Pope et al. (2004)
Iceland geothermal aquifers	30–298	0.001–15	0.3–3770	<0.01–0.38	<0.002–0.8	Kaasalainen et al. (2015)
Reykjanes geothermal aquifer, Iceland	285	9.0	3770	<0.1	0.38	Kaasalainen et al. (2015)
Reykjanes geothermal aquifer, Iceland	279–314 (n = 6)	8.2–12.1	n/a	124–1991	38–491	Hannington et al. (2016)
Kudryavy volcano, Iturup, Kuril Islands	1060–1070	140	n/a	1250	230	Churakov et al. (2000)
Kudryavy volcano, Iturup, Kuril Islands	870	65	n/a	580	5500	Taran et al. (1995)
Fumaroles at La Fossa crater, Vulcano (June 1993)	560	82	n/a	1000	5	Cheynet et al. (2000)
	428	14		2000	12	
	494	16		3200	117	
Tolbachik volcano, Kamchatka (2012–13 eruption)	1060–1070	1700 (400)[a]	1000 (200)[a]	740 (170)[a]	660 (100)[a]	Zelenski et al. (2014)
Tolbachik volcano, Kamchatka (2012–13 eruption)	1030	1470	1700	940	436	Chaplygin et al. (2016)
Mutnovsky volcano, Kamchatka	480	110	1	140	32	Zelenski and Bortnikova (2005)[b]
	507	98	3	130	25	
	410	31	3	25	7	
	450	36	3	40	11	
Kizimen volcano, Kamchatka[c]	210–215	2.9	9.1	14	3.9	Measured for this study[c]
Colima volcano, Mexico	742	24	n/a	451	55	Taran et al. (2001)
	828	53		78	740	
	738	34		480	45	
Kawah Ijen volcano, Indonesia	Up to >450	22	n/a	60	15.1	Berlo et al. (2014)

[a] Means of 14 samples and standard deviation.
[b] Also provide I and Br concentration: 0.35/1.1/1.1/1.7 ppm I; 3.8/3.7/4.0/6.0 ppm Br.
[c] The last major eruption of the Kizimen volcano was in 2010–2011, producing >0.5 km^3 of andesitic lava (Dvigalo et al. 2013). The condensate was collected at 2280 m, October 11–12, 2014; sampling and analysis conditions similar to those of the Avacha sample. The vapor contains 3.30 wt% S, 0.57 wt% Cl, and 3.32 ppm Br.

Fumarole gases from the Avacha volcano were sampled by placing 20 mm diameter quartz tubes in the fumaroles. The tube was connected by a hose made of silicone rubber to two bubblers cooled using a snow-water mixture and connected in series (Fig. 1b). The line was connected to an electric pump, operated at a rate of 1 L/min (see Fig. 3 in Zelenski et al. 2014). The condensates were analyzed by ICP-MS and ICP-AES for trace elements. The chemical analyses of the vapors from the Avacha volcano are shown in Table 8.

The low-temperature, crystalline-sulfur-depositing fluids (≤100 °C) are unusually enriched in Tl (up to 782 ppb). They are also rich in Cd (up to 8230 ppb), compared to exhalations from other volcanoes (Table 7; up to 660 ppb). This unusual enrichment is magnified in the high-temperature vapor (600 °C) condensate, which contains an astonishing 34 ppm Tl, as well as 240 ppm Cd. Iodine was not measured, but the bromine concentration reaches 5 ppm. Other metals (or metalloids) that are highly enriched in this vapor include As, Rb, Ag, In, Sn, Sb, Cs, Mo, and Bi (Table 8).

DISCUSSION

The formation of nataliyamalikite and other Tl minerals associated with the degassing of arc volcanoes reflects the extreme fractionation of Tl during magmatic–hydrothermal processes. Thallium minerals have now been described from rhyolitic (Vulcano, Italy; Campostrini et al. 2008; Cheynet et al. 2000; Demartin et al. 2009; Roberts et al. 2006), andesitic (Avacha; this study) and (alkali) basaltic (Tolbachik, Kamchatka, Russia; Pekov et al. 2015; Siidra et al. 2014a, 2014b, 2014c; Zelenski et al. 2014) volcanoes. In this discussion, first we succinctly review the main processes that cause Tl fractionation and enrichment to levels where minerals containing Tl as an essential element form, and then we discuss the origin of nataliyamalikite in light of this information.

Processes of thallium enrichment and mineralization—A review

Christy (2015) found that 40 out of 70 considered chemical elements displayed a good positive correlation between the crustal abundance of the element and the number of mineral species in which that element is an essential constituent. One of the elements that shows the most dramatic deviation from this trend is Rb, which is hidden in substitution for K, and hence is an essential constituent in only a handful of minerals. Given the similarity of charge and radii between the Tl(I) and Rb(I) ions (1.59 vs. 1.61 Å; Shannon 1976), one may expect a poor diversity of Tl minerals; nevertheless, Tl is one of the 40 elements that follow the main trend defined by Christy (2015). This is because thallium chemistry is more complex than that of Rb [multiple oxidation states; stereochemically active lone pair for the most common oxidation state, Tl(I); chalcophile and lithophile characters], and extreme enrichment of Tl occurs in many environments (Fig. 6) as a result of several different processes, making Tl geochemistry unique (Hettmann et al. 2014), and leading to concentrations of Tl at levels sufficient for it to become an essential component in minerals. Thus, Tl is an example of an element where factors that encourage geochemical dispersal and a low number of species are compensated by factors that would

TABLE 8. Chemical analyses of condensates from Avacha fumaroles collected in May 2016

Element	DL ppb	AC-5 ppb	AC-4 ppb	AC-1 ppb
S	533	9 917 342	9 958 559	11 596 551
Na	184	<DL	1357	5687
Mg	122	<DL	425	440
Al	30	171	254	1118
Si	128	5469	5111	22 258
P	463	<DL	< DL	<DL
K	94	<DL	<DL	4678
Ca	583	2635	2393	3461
Mn	3	<DL	4.1	25.3
Fe	144	<DL	<DL	667
B	16	235	1859	62 065
As	2	<DL	<DL	2854
Br	331	<DL	<DL	5154
Tl	14	211	782	33 836
Se	10	<DL	<DL	149
Sr	2	<DL	<DL	7.6
Ba	3	104	105	1319
Hg	0.4	1.5	<DL	18.3
Pb	1	28.7	11.7	464
Li	182	<DL	1019	2310
Rb	236	<DL	<DL	14 651
Zr	166	783	848	11 569
Ag	734	1628	869	1218
Zn	21	28.2	<DL	124
Cd	172	4000	8230	240 168
In	117	<DL	<DL	4002
Sn	818	<DL	<DL	69 662
Sb	212	<DL	<DL	65 114
Te	225	532	420	15 866
Cs	33	<DL	56.0	8239
Hf	50	<DL	<DL	610
W	138	304	1065	<DL
Mo	293	628	667	2795
Re	15	<DL	<DL	576
Pt	34	<DL	<91	508
Au	41	371	<100	<DL
Bi	25	144	92.3	5131
U	28	<DL	<DL	45.5

Notes: Samples AC-5 and AC-4 are from low-temperature gas condensates (*T* ~100 °C) associated with native sulfur deposition, and sample AC-1 was taken from the same fumarole that deposits nataliyamalikite; vapor temperature was ~600 °C (Fig. 1b). DL = detection limits. The following elements were below DL in all three samples: Sc <2 ppb; Ti <24 ppb; V <3 ppb; Cr <27 ppb; Co <4 ppb; Ni <7 ppb; Cu <11 ppb; Ga <2 ppb; Ge <2 ppb; Be <206 ppb; Y <193 ppb; Nb <151 ppb; Ru <106 ppb; Rh <145 ppb; Pd <156 ppb; La <102 ppb; Ce <29 ppb; Pr <26 ppb; Nd <77 ppb; Sm <51 ppb; Eu <21 ppb; Gd <19 ppb; Tb <10 ppb; Dy <19 ppb; Ho <8 ppb; Ho <8 ppb; Er <50 ppb; Tm <5 ppb; Yb <25 ppb; Lu <4 ppb; Ta <44 ppb; Os <23 ppb; Ir <13 ppb; Th <32 ppb.

normally generate a superabundance of species (Christy 2015), leading to the apparent "normal trend" behavior that is observed. To date >65 minerals with Tl as an essential component have been described, compared to just 3 Rb minerals, despite the low crustal abundance of Tl (550 ppb) compared to Rb (90 ppm).

The key processes involved in enriching Tl are (see also Fig. 6):

(1) Magma incompatibility. The solar system abundance of Tl is 142 ppb (Anders and Grevese 1989), yet mantle abundance is only ~3 ppb. This strong mantle depletion is primarily due to the volatile nature of Tl; volatile elements are depleted in the Earth and other rocky planets due to the high temperature and violent processes active during planetary growth (e.g., O'Neill and Palme 2008). However, Tl behaves as a highly incompatible element in silicate magmatic systems (Shaw 1952), and so a component of the mantle depletion reflects its partitioning into the crust. Thallium concentrations increase via magmatic differentiation, reaching hundreds of parts per billion in the
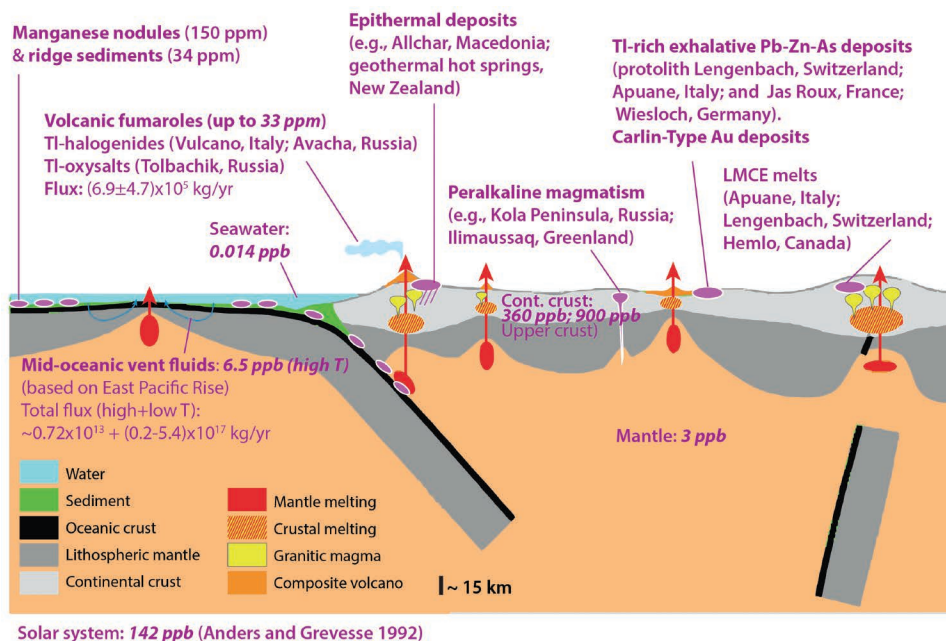
FIGURE 6. Schematic view of thallium cycling and the geotectonic location of deposits containing Tl-minerals. Background images from http://minerva.union.edu/hollochk/kth/illustrations.html. (Color online.)

continental crust. Extreme Tl enrichment via magmatic differentiation occurs in some highly evolved magmatic systems, most notably peralkaline magmatism (e.g., Lovozero and Khibina massifs, Kola Peninsula, Russia; Ilimaussaq, Greenland), where late magmatic activity results in widespread formation of Tl-rich sulfide assemblages (Hettmann et al. 2014; Pekov and Agakhanov 2009).

(2) Hydrothermal transport and deposition. Thallium exhibits both lithophile and chalcophile behaviors; as a chalcophile element, it forms numerous hydrothermal sulfide and sulfosalt minerals. Thallium is transported as chloride complexes (Bebie et al. 1998) and possibly bisulfide complexes (Xiong 2007) in hydrothermal fluids (Brugger et al. 2016), and large Tl concentrations are associated with hydrothermal, sulfide-rich deposits. Thallium is recovered primarily as a by-product of Zn smelting (thallium sits within the sphalerite structure; Xiong 2007), but only a few hydrothermal Zn deposits contain Tl-bearing minerals (e.g., Wiesloch, Germany; Seeliger 1963). Spectacular Tl enrichment associated with a complex mineralogy are found in some As-rich volcanogenic hydrothermal deposits (e.g., Allchar, Macedonia; Amthauer et al. 2012; Jankovic and Jelenkovic 1994; Volkova et al. 2006) and in Carlin-type gold deposits in Nevada, U.S.A. (Large et al. 2011; Muntean et al. 2011). Scale deposits in boreholes and hot spring deposits from active geothermal fields provide a modern analog for such hydrothermal Tl enrichment, as they contain up to 1000 ppm Tl (Weissberg 1969). Note that these enrichments do not require highly enriched fluids; for example the Champagne Pool sediments in New Zealand contain >300 ppm Tl (Weissberg 1969), but the waters carry only 27 ppt Tl (Pope et al. 2004). At Vulcano, Italy, fumarolitic fluids carry 14–82 ppb Tl (Table 7; Cheynet et al. 2000), but altered rocks

around the fumaroles carry more than three orders of magnitude more Tl (up to 280 ppm Tl; Boyce et al. 2007; Fulignati and Sbrana 1998). This highlights the importance of deposition mechanisms in controlling Tl enrichment (e.g., evaporation; coprecipitation or sorption—see also process 3).

(3) Sorption and oxidation. Nielsen et al. (2006b) used chemical and isotopic mass-balance calculations to estimate the hydrothermal flux of Tl from oceanic crust into oceans at ~0.72 $\times 10^{13}$ kg/yr from high-temperature fluids, and (0.2–5.4) $\times 10^{17}$ kg/yr from low-temperature fluid seepage at ridge flanks. Much of this Tl is retained in oceanic sediments (34 ppm Tl in ridge sediments), with extreme enrichments (150 ppm on average) in ferromanganese nodules (Fig. 6). Thallium(I) is the only oxidation state relevant for magmatic and hydrothermal processes, but Peacock and Moon (2012) showed that Tl(I) species are oxidized to insoluble Tl(III) following sorption onto hexagonal birnessite. The magnitude of this process and the association with a strong isotopic fractionation compared to magmatic and hydrothermal processes make thallium a diagnostic element for deep marine sediments, to such an extent that addition of minor amounts of Mn-rich crusts into the mantle can explain the pronounced thallium-isotope variations recorded in ocean–island basalts (Nielsen et al. 2006a, 2006b).

(4) Low melting point assemblages. Partial melting of sulfide ores can generate melts that are highly enriched in low melting point chalcophile (LMPC) elements and precious metals such as Tl, As, Sb, Bi, Te, Pb, Ag, and Au (Frost et al. 2002; Tomkins et al. 2007); upon cooling these melts can crystallize several unusual sulfosalt minerals, including many Tl minerals (Frost et al. 2002; Tomkins and Mavrogenes 2002). LMPC melts can also precipitate directly from hydrothermal fluids via reaction mechanisms such as fluid-rock interaction (Tooth et

al. 2008, 2011). An important part of the melting and fractional cooling process is that a series of steps results in progressive enrichment of the elements with greatest tendency to stay in the lowest temperature sulfosalt melts, of which Tl may have the most pronounced proclivity: melts persist to <275 °C along the Tl_2S-As_2S_3 joint, for example (Tomkins et al. 2004). Well-studied examples of partial melting leading to extreme local enrichment in Tl include sediment-hosted base metal deposits such as the Lengenbach Pb-Zn-As-Tl-Ba deposit, Switzerland (Hofmann and Knill 1996); Jas Roux, French Alps (Johan and Mantienne 2000); and the Monte Arsiccio mine (Alpi Apuane, Tuscany, Italy) (Biagioni et al. 2013); as well as the shear-hosted Hemlo gold deposit, Canada (Harris 1989; Tomkins et al. 2004).

(5) Volatile. As mentioned above, it is well known that Tl and Cd are volatile, being discharged in high-temperature magmatic vapors (Henley and Berger 2013). This behavior was confirmed experimentally by Johnson and Canil (2011). Baker et al. (2009) estimated the Tl flux from subaerial volcanoes at $(6.9 \pm 4.7) \times 10^5$ kg/yr. The composition of the fumaroles from Avacha (34 ppm Tl), and of the magmatic vapors (>1000 °C) from the 2012–2013 Tolbachik eruption (~1500 ppm Tl) highlight the fact that vapor partitioning itself can lead to the formation of highly enriched fluids, which may become supersaturated with Tl minerals via cooling, fluid mixing, or fluid-rock interaction.

Formation of nataliyamalikite

Nataliyamalikite is defined as the orthorhombic form of TlI. Given the melting point of TlI (442 °C) and arsenic sulfides (<321 °C), and the high-temperature deposition in the fumarolic environment (~600 °C), it is possible that droplets of Tl-, As- and halogen-rich liquid were first condensed from vapor (Mavrogenes et al. 2010), before crystallization of the cubic polymorph of nataliyamalikite (Fig. 2a) and associated minerals upon cooling. On the other hand, the rare occurrence of natali-yamalikite on mascagnite (Fig. 3) suggests that, at least for this sample, the condensation temperature was less than 400 °C and perhaps even as low as 250 °C.

The observation of the pseudo-cubic morphology of most nataliyamalikite crystals supports initial crystallization of the high-temperature cubic polymorph, the present predominant orthorhombic structure resulting from phase transformation after cooling below 175 °C. Under laboratory conditions, the high temperature, cubic polymorph usually transforms rapidly into the orthorhombic form upon cooling. However, Brightwell et al. (1983) found that the quenching properties of pure cubic TlI are dependent upon the crystal's thermal history:

> Attempts to quench in the high-temperature form of TlI by rapid cooling to –196 °C failed, but it was found that after repeated runs in the differential scanning calorimeter, TlI showed a sharp transition at 175 °C; after thermal soaking at 200 °C, to eliminate completely the low-temperature form, the reverse transition did not occur during cooling, at a rate of 8 K min^{-1}, to room temperature. The high-temperature red form then took several weeks to undergo a complete transition to the yellow form at room temperature.

The coexistence of the orthorhombic and cubic modifications of TlI can be explained three-ways: (1) the addition of minor amounts of elements such as Br and Ag have been shown to extend the stability of the cubic form (Brightwell et al. 1983); (2) the cubic form can also be synthesized at low temperature (<15 °C) via vapor deposition on amorphous surfaces (Black-man and Khan 1960); (3) slow transformation of the cubic to orthorhombic forms after the samples were collected.

As illustrated in Figure 2a, many vacuoles in the amorphous S-rich matrix contain nano-crystals of nataliyamalikite. This is suggestive of direct condensation of the nataliyamalikite precursor phase from the vapor. A simple mass-balance calculation suggests that the size and distribution of the nataliyamalikite nanocrystals are consistent with the measured Tl concentrations in the vapor (34 ppm): a 10 nm nataliyamalikite crystal can form from the vapor contained within a 6 μm radius bubble. The observed radii of the vapor bubbles are mostly between 4 and 5 μm, and many contain 10–50 nm nataliyamalikite crystals. The larger crystals (exceptionally up to nearly 1 μm in size) most likely reflect the difficulty of nucleating nataliyamalikite (i.e., a nataliyamalikite crystal will not nucleate in every vacuole).

Origin of the Tl-rich fumarolitic fluids

The enrichment of Tl to 10–100 ppb levels in gases resulting from the shallow degassing of magmas has been recognized for a long time (e.g., Fulignati and Sbrana 1998; Table 7). However, the 2012–2013 basaltic Tolbachik eruption provided the first evidence for extreme Tl enrichment in Cl-rich magmatic vapors (to ~1.5–2.0 ppm; Chaplygin et al. 2016; Zelenski et al. 2014; Table 7). Avacha represents a new example of extreme Tl enrichment in gasses from degassing magmas. Even the low-temperatures fumarolitic fluids display record Tl contents (to 782 ppb), with the condensates from high-temperature fumaroles containing 34 ppm Tl. At least some of the nataliyamalikite crystals clearly formed directly from the vapor during cooling (Fig. 2a). Deeper within the fumarolic system, repeated periods of greater and lesser vapor flux would promote refinement of element distribution. The more volatile elements like Tl and As would be concentrated at higher levels in the system; hence, deposition of LMPC assemblages [As-Se-Te-Tl-Bi-(Pb)] at shallow depth is likely. The precious metals (Ag, Au, Re) would be concentrated at the first appearance of liquid sulfosalts (Tooth et al. 2011). We suggest that interaction between the liquid sulfosalts (containing wt% levels of Tl) and magmatic vapors can explain the extremely high-Tl concentrations in the high-T fumaroles at Avacha.

IMPLICATIONS

The determination of the nataliyamalikite structure in this study demonstrates the value of combining FIB-SEM techniques for in situ extraction of small volumes of well-characterized material from the surface of a polished section for single-crystal X-ray analysis using synchrotron radiation, in combination with SEM-based EBSD to provide some statistics on the nature of the grains affected by potential polymorphism.

The formation of Tl minerals such as nataliyamalikite from active fumaroles provides a vivid illustration of the role of subduction and arc-related volcanism as "Nature's refineries"

(Henley and Berger 2013) (Fig. 6). The mechanisms that result in enrichment of Tl by 4 orders of magnitude from the mantle source (3 ppb) to a magmatic vapor (33 ppm) are complex, involving hydrothermal leaching of Tl(I), concentration via oxidation to immobile Tl(III) on the surface of deep-sea Mn minerals, partial melting of the Tl-rich subducted source, and complex vapor-liquid sulfosalt-fluid-solid equilibria during the fumarolitic stage of the volcanic eruption.

The high-temperature fumarolitic fluids from Avacha not only contain >400× more Tl than the Vulcano fumaroles (that also deposit Tl minerals), they are also highly enriched in As, Sb, Cd, Re, and Te (Table 8). The processes that led to the formation of nataliyamalikite illustrate the ability of low-density vapors to carry significant amounts of metals (e.g., Hurtig and Williams-Jones 2015), and also provide an insight into the processes that can lead to the formation of fluids with extreme metal contents. In this case, we hypothesize that the interaction between vapors and melts was the main factor at work: (1) at a shallow depth (vapor stable) in the geothermal system below the Avacha volcanic edifice, sulfosalt melts rich in As, Se, Te, and Tl interact with vapor and enrich it in these elements. A vertically extensive (from summit at 2741 to −1000 m altitude) geothermal reservoir characterized by mixing of magmatic water and volatiles with surface waters (glacier melting) has been delineated on the basis of seismicity underneath the Avacha volcano (Kiryukhin et al. 2015). (2) Cooling of Tl-rich vapor bubbles near the surface allows direct condensation of TlI, either as melt droplets or as the cubic form of TlI. These eventually convert to nataljamalikiite on cooling. This is in contrast to the occurrence of Tl minerals at Vulcano, for example, where the fumarolitic fluids do not display extreme enrichment in Tl, and Tl is concentrated via depositional processes to levels conducive to the formation of Tl minerals. The processes that result in extreme enrichment of Tl (and other volatile metals and semi-metals) in vapors are obviously transient and rarely preserved; however, these processes may be important in controlling the distribution of these metals in vapor-dominated epithermal systems.

REFERENCES CITED

Amthauer, G., Pavicevic, M.K., Jelenkovic, R., El Goresy, A., Boev, B., and Lazic, P. (2012) State of geoscientific research within the lorandite experiment (LOREX). Mineralogy and Petrology, 105, 157–169.

Anders, E., and Grevese, N. (1989) Abundances of the elements: Meteoritic and solar. Geochimica et Cosmochima Acta, 53, 197–214.

Baker, R.G.A., Rehkaemper, M., Hinkley, T.K., Nielsen, S.G., and Toutain, J.P. (2009) Investigation of thallium fluxes from subaerial volcanism-Implications for the present and past mass balance of thallium in the oceans. Geochimica et Cosmochimica Acta, 73, 6340–6359.

Bebie, J., Seward, T.M., and Hovey, J.K. (1998) Spectrophotometric determination of the stability of thallium(I) chloride complexes in aqueous solutions up to 200 °C. Geochimica et Cosmochimica Acta, 62, 1643–1651.

Berlo, K., van Hinsberg, V.J., Vigouroux, N., Gagnon, J.E., and Williams-Jones, A.E. (2014) Sulfide breakdown controls metal signature in volcanic gas at Kawah Ijen

volcano, Indonesia. Chemical Geology, 371, 115–127.

Biagioni, C., D'Orazio, M., Vezzoni, S., Dini, A., and Orlandi, P. (2013) Mobilization of Tl-Hg-As-Sb-(Ag,Cu)-Pb sulfosalt melts during low-grade metamorphism in the Alpi Apuane (Tuscany, Italy). Geology, 747–750.

Bindeman, I.N., Vinogradov, V.I., Valley, J.W., Wooden, J.L., and Natal'in, B.A. (2002) Archean protolith and accretion of crust in Kamchatka: SHRIMP dating of zircons from Sredinny and Ganal Massifs. Journal of Geology, 110, 271–289.

Blackman, M., and Khan, I.H. (1960) The polymorphism of thallium and other halides at low temperatures. Proceedings of the Physical Society, 77, 471–475.

Boyce, A.J., Fulignati, P., Sbrana, A., and Fallick, A.E. (2007) Fluids in early stage hydrothermal alteration of high-sulfidation epithermal systems: A view from the Vulcano active hydrothermal system (Aeolian Island, Italy). Journal of Volcanology and Geothermal Research, 166, 76–90.

Brightwell, J.W., Miller, L.S., Munday, A., and Ray, B. (1983) The silver iodide-thallium iodide pseudo-binary system. Physica status solidi (a), 79, 293–300.

Brugger, J., Liu, W., Etschmann, B., Mei, Y., Sherman, D.M., and Testemale, D. (2016) A review of the coordination chemistry of hydrothermal systems, or do coordination changes make ore deposits? Chemical Geology, 447, 219–253.

Campostrini, I., Demartin, F., Gramaccioli, C.M., and Orlandi, P. (2008) Hephaistosite, TlPb₂Cl₅, a new thallium mineral species from La Fossa crater, Vulcano, Aeolian Islands, Italy. Canadian Mineralogist, 46, 701–708.

Chaplygin, I.V., Lavrushin, V.Y., Dubinina, E.O., Bychkova, Y.V., Inguaggiato, S., and Yudovskaya, M.A. (2016) Geochemistry of volcanic gas at the 2012-13 New Tolbachik eruption, Kamchatka. Journal of Volcanology and Geothermal Research, 323, 186–193.

Cheynet, B., Dall'Aglio, M., Garavelli, A., Grasso, M.F., and Vurro, F. (2000) Trace elements from fumaroles at Vulcano Island (Italy): Rates of transport and a thermo-chemical model. Journal of Volcanology and Geothermal Research, 95, 273–283.

Christy, A.G. (2015) Causes of anomalous mineralogical diversity in the Periodic Table. Mineralogical Magazine, 79, 33–49.

Churakov, S.V., Tkachenko, S.I., Korzhinskii, M.A., Bocharnikov, R.E., and Shmulo-vich, K.I. (2000) Evolution of composition of high-temperature fumarolic gases from Kudryavy volcano, Iturup, Kuril Islands: The thermodynamic modeling. Geochemistry International, 38, 436–451.

Ciobanu, C.L., Brugger, J., Cook, N.J., Mills, S.J., Elliott, P., Damian, G., and Damian, F. (2014) Gratianite, MnBi₂S₄, a new mineral from the Baita Bihor skarn, Romania. American Mineralogist, 99, 1163–1170.

Demartin, F., Gramaccioli, C.M., and Campostrini, I. (2009) Steropesite, Tl₃BiCl₆, a new thallium bismuth chloride from La Fossa Crater, Vulcano, Aeolian Islands, Italy. Canadian Mineralogist, 47, 373–380.

Dvigalo, V.N., Melekestsev, I.V., Shevchenko, A.V., and Svirid, I.Y. (2013) The 2010-2012 eruption of Kizimen Volcano: The greatest output (from the data of remote-sensing observations) for eruptions in Kamchatka in the early 21st century part I. The November 11, 2010 to December 11, 2011 phase. Journal of Volcanology and Seismology, 7, 345–361.

Fulignati, P., and Sbrana, A. (1998) Presence of native gold and tellurium in the active high-sulfidation hydrothermal system of the La Fossa volcano (Vulcano, Italy). Journal of Volcanology and Geothermal Research, 86, 187–198.

Frost, B.R., Mavrogenes, J.A., and Tomkins, A.G. (2002) Partial melting of sulfide ore deposits during medium and high grade metamorphism. Canadian Mineralo-gist, 40, 1–18.

Gorshkov, A.I., Vinokurov, S.F., Solodov, D.I., Bershov, L.V., Mokhov, A.V., Solodova, Y.P., and Sivtsov, A.V. (1998) Polycrystalline diamond from the Udachnaya pipe, Yakutia: Mineralogical, geochemical, and genetic characteristics. Lithology and Mineral Resources, 33, 525–538.

Hannington, M., Harðardóttir, V., Garbe-Schönberg, D., and Brown, K.L. (2016) Gold enrichment in active geothermal systems by accumulating colloidal suspensions. Nature Geoscience, 9, 299–302.

Harris, D.C. (1989) The mineralogy and geochemistry of the Hemlo gold deposit, Ontario. Geological Survey of Canada Economic Geology Report, 38, 88 pp.

Helmholz, L. (1937) The crystal structure of the low temperature modification of thal-lous iodide. Zeitschrift für Kristallographie—Crystalline Materials, 95, 129–137.

Henley, R.W., and Berger, B.R. (2013) Nature's refineries—Metals and metalloids in arc volcanoes. Earth-Science Reviews, 125, 146–170.

Hettmann, K., Marks, M.A.W., Kreissig, K., Zack, T., Wenzel, T., Rehkaemper, M., Jacob, D.E., and Markl, G. (2014) The geochemistry of Tl and its isotopes during magmatic and hydrothermal processes: The peralkaline Ilimaussaq complex, southwest Greenland. Chemical Geology, 366, 1–13.

Hofmann, B.A., and Knill, M.D. (1996) Geochemistry and genesis of the Lengenbach Pb-Zn-As-Tl-Ba-mineralisation, Binn Valley, Switzerland. Mineralium Deposita, 31, 319–339.

Hu, Z., and Gao, S. (2008) Upper crustal abundances of trace elements: A revision and update. Chemical Geology, 253, 205–221.

Hurtig, N.C., and Williams-Jones, A.E. (2015) Porphyry-epithermal Au-Ag-Mo ore formation by vapor-like fluids: New insights from geochemical modeling. Geol-ogy, 43, 587–590.

Ivanov, B.V., Flerov, G.B., Masurenkov, Y.P., Kirianov, V.Y., Melekestsev, I.V., Taran, Y.A., and Ovsiannikov, A.A. (1996) The 1991 eruption of Avacha Volcano: Dynamics and composition of eruptive products. Journal of Volcanology and

Seismology, 17, 369–394.

Jankovic, S., and Jelenkovic, R. (1994) Thallium mineralization in the Allchar Sb-As-Tl-Au Deposit. Neues Jahrbuch für Mineralogie-Abhandlungen, 167, 283–297.

Johan, Z., and Mantienne, J. (2000) Thallium-rich mineralization at Jas Roux, Hautes-Alpes, France: A complex epithermal, sediment-hosted, ore-forming system. Journal of the Czech Geological Society, 45, 63–77.

Johnson, A., and Canil, D. (2011) The degassing behavior of Au, Tl, As, Pb, Re, Cd and Bi from silicate liquids: Experiments and applications. Geochimica et Cosmochimica Acta, 75, 1773–1784.

Kaasalainen, H., Stefánsson, A., Giroud, N., and Arnórsson, S. (2015) The geochemistry of trace elements in geothermal fluids, Iceland. Applied Geochemistry, 62, 207–223.

Kiessling, R. (1949) The binary system chromium-boron .1. Phase analysis and structure of the zeta-phase and theta-phase. Acta Chemica Scandinavica, 3, 595–602.

Kiryukhin, A., Manukhin, Y., Fedotov, S., Lavrushin, B., Rychkova, T., Ryabinin, G., Polyakov, A., and Voronin, P. (2015) Geofluids of Avachinsky-Koryaksky Volcanogenic Basin, Kamchatka, Russia. Proceedings World Geothermal Congress 2015 Melbourne, Australia, 19-25 April 2015, 11 pp.

Koulakova, I., Jaxybulatova, K., Shapiroc, N.M., Abkadyrova, I., Deeva, E., Jakovleva, A., Kuznetsova, P., Gordeevd, E., and Chebrove, V. (2014) Asymmetric caldera-related structures in the area of the Avacha group of volcanoes in Kamchatka as revealed by ambient noise tomography and deep seismic sounding. Journal of Volcanology and Geothermal Research, 285, 36–46.

Large, R.R., Bull, S.W., and Maslennikov, V.V. (2011) A carbonaceous sedimentary source-rock model for Carlin-type and orogenic gold deposits. Economic Geology, 106, 331–358.

Léger, J.M., Haines, J., Danneels, C., and de Oliveira, L.S. (1998) The TlI-type structure of the high-pressure phase of NaBr and NaI; pressure-volume behaviour to 40 GPa. Journal of Physics-Condensed Matter, 10, 4201–4210.

Levin, V., Droznin, D., Park, J., and Gordeev, E. (2004) Detailed mapping of seismic anisotropy with local shear waves in southeastern Kamchatka. Geophysical Journal International, 158, 1009–1023.

Li, Y.-H. (1991) Distribution patterns of the elements in the ocean: A synthesis. Geochimica Cosmochima Acta, 55, 3223–3240.

Mavrogenes, J.A., Henley, R.W., Reyes, A.G., and Berger, B. (2010) Sulfosalt melts: Evidence of high-temperature vapor transport of metals in the formation of high-sulfidation lode gold deposits. Economic Geology, 105, 257–262.

McGimsey, R.G., Neal, C.A., and Girina, O. (2004) 2001 Volcanic activity in Alaska and Kamchatka: Summary of events and response of the Alaska Volcano Observatory. USGS Open-File Report 2004-1453, 53 pp.

Melekestsev, I.V., Braitseva, O.A., Dvigalo, V.N., and Bazanova, L.I. (1994) Historical eruptions of the Avacha Volcano, Kamchatka. Attempt of modern interpretation and classification for long-term prediction of the types and parameters of future eruptions. Part 2 (1926–1991). Journal of Volcanology and Seismology, 16, 93–114.

Moiseenko, K.B., and Malik, N.A. (2014) Estimates of total ash content from 2006 and 2009 explosion events at Bezymianny volcano with use of a regional atmospheric modeling system. Journal of Volcanological and Geothermal Research, 270, 53–75.

Muntean, J.L., Cline, J.S., Simon, A.C., and Longo, A.A. (2011) Magmatic-hydrothermal origin of Nevada's Carlin-type gold deposits. Nature Geoscience, 4, 122–127.

Nielsen, S.G., Rehkamper, M., Norman, M.D., Halliday, A.N., and Harrison, D. (2006a) Thallium isotopic evidence for ferromanganese sediments in the mantle source of Hawaiian basalts. Nature, 439, 314–317.

Nielsen, S.G., Rehkamper, M., Teagle, D.A.H., Butterfield, D.A., Alt, J.C., and Halliday, A.N. (2006b) Hydrothermal fluid fluxes calculated from the isotopic mass balance of thallium in the ocean crust. Earth and Planetary Science Letters, 251, 120–133.

O'Neill, H.St.C., and Palme, H. (2008) Collisional erosion and the non-chondritic composition of the terrestrial planets. Philosophical Transactions of the Royal Society A, 366, 4205–4238.

Peacock, C.L., and Moon, E.M. (2012) Oxidative scavenging of thallium by birnessite: Explanation for thallium enrichment and stable isotope fractionation in marine ferromanganese precipitates. Geochimica et Cosmochimica Acta, 84, 297–313.

Pedoja, K., Bourgeois, J., Pinegina, T., and Higman, B. (2006) Does Kamchatka belong to North America? An extruding Okhotsk block suggested by coastal neotectonics of the Ozernoi Peninsula, Kamchatka, Russia. Geology, 34, 353–356.

Pekov, I.V., and Agakhanov, A.A. (2009) Thallium-rich murunskite from the Lovozero pluton, Kola Peninsula, and partitioning of alkali metals and thallium between sulfide minerals. Geology of Ore Deposits, 50, 583–589.

Pekov, I.V., Zubkova, N.V., Belakovskiy, D.I., Yapaskurt, V.O., Vigasina, M.F., Lykova, I.S., Sidorov, E.G., and Pushcharovsky, D.Y. (2015) Chrysothallite $K_6Cu_6Tl^{3+}Cl_{17}(OH)_4 \cdot H_2O$, a new mineral species from the Tolbachik volcano, Kamchatka, Russia. Mineralogical Magazine, 79, 365–376.

Pope, J.G., McConchie, D.M., Clark, M.D., and Brown, K.L. (2004) Diurnal variations in the chemistry of geothermal fluids after discharge, Champagne Pool, Waiotapu, New Zealand. Chemical Geology, 203, 253–272.

Roberts, A.C., Venance, K.E., Seward, T.M., Grice, J.D., and Paar, W.H. (2006) Lafossaite. A new mineral from the La Fossa Crater, Vulcano, Italy. Mineralogical Magazine, 37, 165–168.

Samara, G.A., Walters, L.C., and Northrop, D.A. (1967) Polymorphism compressibility and thermal expansion of thallous iodide. Journal of Physics and Chemistry of Solids, 28, 1875–1883.

Seeliger, E. (1963) Die Paragenese der Pb-Zn-Erzlagerstätten am Gänsberg bei Wiesloch (Baden) und ihre genetischen Beziehungen zu den Gängen im Odenwaldkristallin, zu Altwiesloch und der Vererzung der Trias des Kraichgau. Jahreshefte des Geologischen Landesamtes in Baden-Württemberg, 6, 239–299.

Shamovskii, L.M., and Shushkanov, A.D. (1968) Crystallochemical laws of the formation of spectometric scintillators based on alkali-halide crystals. Doklady Akademii Nauk SSSR, 181, 862–865.

Shannon, R.D. (1976) Revised effective ionic radii and systematic studies of interatomic distances in halides and chalcogenides. Acta Crystallographica, A32, 751–767.

Shaw, D.M. (1952) The geochemistry of thallium. Geochimica et Cosmochimica Acta, 2, 118–154.

Sheldrick, G.M. (2008) A short history of SHELX. Acta Crystallographica, A64, 112–122.

Siidra, O.I., Vergasova, L.P., Kretser, Y.L., Polekhovsky, Y., Filatov, S.K., and Krivovichev, S.P. (2014a) Unique thallium mineralization in the fumaroles of Tolbachik volcano II. Karpovite, $Tl_2VO(SO_4)_2(H_2O)$. Mineralogical Magazine, 78, 1699–1709.

——— (2014b) Unique thallium mineralization in the fumaroles of Tolbachik volcano, Kamchatka, Russia. III. Evdokimovite, $Tl_4(VO)_3(SO_4)_5(H_2O)_5$. Mineralogical Magazine, 78, 1711–1724.

Siidra, O.I., Vergasova, L.P., Krivovichev, S.P., Kretser, Y.L., Zaitsev, A.N., and Filatov, S.K. (2014c) Unique thallium mineralization in the fumaroles of Tolbachik volcano, Kamchatka Peninsula, Russia. I. Markhininite, $TlBi(SO_4)_2$. Mineralogical Magazine, 78, 1687–1698.

Simmons, S.F., Brown, K.L., and Tutolo, B.M. (2016) Hydrothermal transport of Ag, Au, Cu, Pb, Te, Zn, and other metals and metalloids in New Zealand geothermal systems: Spatial patterns, fluid-mineral equilibria, and implications for epithermal mineralization. Economic Geology, 111, 589–618.

Taran, Y.A., Hedenquist, J.W., Korzhinsky, M.A., Tkachenko, S.I., and Shmulovich, K.I. (1995) Geochemistry of Magmatic Gases From Kudryavy Volcano, Iturup, Kuril Islands. Geochimica et Cosmochimica Acta, 59, 1749–1761.

Taran, Y.A., Connor, C.B., Shapar, V.N., Ovsyannikov, A.A., and Bilichenko, A.A. (1997) Fumarolic activity of Avachinsky and Koryaksky volcanoes, Kamchatka, from 1993 to 1994. Bulletin of Volcanology, 58, 441–448.

Taran, Y.A., Bernard, A., Gavilanes, J.-C., Lunezheva, E., Cortés, A., and Armienta, M.A. (2001) Chemistry and mineralogy of high-temperature gas discharges from Colima volcano, Mexico. Implications for magmatic gas-atmosphere interaction. Journal of Volcanological and Geothermal Research, 108, 245–264.

Tomkins, A.G., and Mavrogenes, J.A. (2002) Mobilization of gold as a polymetallic melt during pelite anatexis at the Challenger deposit, South Australia: A metamorphosed Archean gold deposit. Economic Geology and the Bulletin of the Society of Economic Geologists, 97, 1249–1271.

Tomkins, A.G., Pattison, D.R.M., and Zaleski, E. (2004) The Hemlo gold deposit, Ontario: An example of melting and mobilization of a precious metal-sulfosalt assemblage during amphibolite facies metamorphism and deformation. Economic Geology, 99, 1063–1084.

Tomkins, A.G., Pattison, D.R.M., and Frost, B.R. (2007) On the initiation of metamorphic sulfide anatexis. Journal of Petrology, 48, 511–535.

Tooth, B.A., Brugger, J., Ciobanu, C., and Liu, W. (2008) Modeling of gold scavenging by bismuth melts coexisting with hydrothermal fluids. Geology, 36, 815–818.

Tooth, B., Ciobanu, C.L., Green, L., O'Neill, B., and Brugger, J. (2011) Bi-melt formation and gold scavenging from hydrothermal fluids: An experimental study. Geochimica et Cosmochimica Acta, 75, 5423–5443.

Viccaro, M., Giuffrida, M., Nicotra, E., and Ozerov, A.Y. (2012) Magma storage, ascent and recharge history prior to the 1991 eruption at Avachinsky Volcano, Kamchatka, Russia: Inferences on the plumbing system geometry. Lithos, 140-141, 11–24.

Volkova, A.V., Serafimovskib, T., Kochnevaa, N.T., Tomsona, I.N., and Tasevb, G. (2006) The Alshar Epithermal Au–As–Sb–Tl Deposit, Southern Macedonia. Geology of Ore Deposits, 48, 175–192.

Waltham, T. (2001) A guide to the volcanoes of southern Kamchatka, Russia. Proceedings of the Geologists' Association, 112, 67–78.

Weissberg, B.G. (1969) Gold-silver ore-grade precipitates from New Zealand thermal waters. Economic Geology, 64, 95–108.

Xiong, Y. (2007) Hydrothermal thallium mineralization up to 300 °C: A thermodynamic approach. Ore Geology Reviews, 32, 291–313.

Zelenski, M., and Bortnikova, S. (2005) Sublimate speciation at Mutnovsky volcano, Kamchatka. European Journal of Mineralogy, 17, 107–118.

Zelenski, M., Malik, N., and Taran, Y. (2014) Emissions of trace elements during the 2012–2013 effusive eruption of Tolbachik volcano, Kamchatka—enrichment factors, partition coefficients and aerosol contribution. Journal of Volcanology and Geothermal Research, 285, 136–149.